CrystEngComm

Accepted Manuscript

ROYAL SOCIETY OF CHEMISTRY

www.rsc.org/crystengcomm

Thermodynamics by synchrotron X-ray Diffraction: Phase relationships and crystal structure of L-tyrosine ethyl ester form III

Béatrice Nicolaï[1], Jean-Paul Itié[2], Maria Barrio[3], Josep-Lluis Tamarit[3], Ivo B. Rietveld[1]

[1] Caractérisation des Matériaux Moléculaires à Activité Thérapeutique (CAMMAT), Faculté de Pharmacie, Université Paris Descartes, 4, Avenue de l'Observatoire, 75006, Paris, France

[2] Beamline Psiché, Synchrotron SOLEIL - L'Orme des Merisiers Saint-Aubin - BP 48 91192 Gif-sur-Yvette, France

[3] Grup de Caracterització de Materials (GCM), Departament de Física i Enginyeria Nuclear, Universitat Politècnica de Catalunya, ETSEIB, Diagonal 647, 08028 Barcelona, Catalonia, Spain

Abstract

In the case of small organic molecules, phase behaviour, important for pharmaceutical applications, is often only studied as a function of temperature. However, for a full thermodynamic description not only the temperature but also the pressure should be taken into account, because pressure and temperature are the two characteristic variables for the Gibbs energy. The commercial form of L-tyrosine ethyl ester has been studied by synchrotron X-ray diffraction while subjected to different pressures and temperatures. At room temperature, it turns into a new previously unknown form around 0.45 GPa. The structure has been solved with an orthorhombic unit cell, space group $P2_12_12_1$, with parameters a = 12.655(4) Å, b = 16.057(4) Å, c = 5.2046(12) Å, and V = 1057.6(5) Å^3 at T = 323 K and P = 0.58 GPa. The enthalpy of the transition from the commercial form into the new form could be estimated from the slope of the transition obtained from the synchrotron diffraction data. In addition, the topological pressure-temperature phase diagram has been constructed involving the two solid phases, the liquid and the vapour phase. The solid phases are enantiotropic under low pressure, but the system becomes monotropic at high pressure with the new solid phase the only stable one.

Keywords: X-ray powder diffraction, calorimetry, phase diagram, stability hierarchy, topological method.

Introduction

Phase stability hierarchy and the construction of phase diagrams by the topological method

For polymorphic substances, crystal structure determination of the different solid phases is only part of the problem. Once a crystal structure is known, its stability in relation to the other polymorphs of the same substance needs to be determined, in particular for pharmaceutical applications.[1] The topological construction of pressure-temperature phase diagrams has recently been established as a reliable method to interpret the phase behaviour of dimorphic systems and to determine the conditions for which the given phases are stable.[2-9]

The topological method is based on determining the effect of pressure and temperature on phase equilibria through the Clapeyron equation:

$$\frac{dP}{dT} = \frac{\Delta S}{\Delta V} = \frac{\Delta H}{T\Delta V} \qquad \text{(Eq. 1)}$$

dP/dT is the slope of a given phase equilibrium in the pressure-temperature phase diagram, ΔS is the entropy change associated to the phase change, and ΔV is the volume change. ΔS equals $\Delta H/T$ (the enthalpy change of the transition divided by the transition temperature) at equilibrium (because ΔG = 0); this equality is therefore valid on the entire equilibrium curve.

In most cases the enthalpy change is determined by calorimetric measurements and the volume changes by X-ray powder diffraction. However, it is often difficult to determine the density (or inversely the specific volume) of the liquid phase; thus in such cases approximations are necessary to determine the slopes and coordinates of, in particular, solid-liquid equilibria in a phase diagram. However, statistical averages of liquid densities of small organic molecules with respect to their solid phases and of the volume

change of the liquid phase as a function of temperature lead to acceptable results.[10,11] A number of phase diagrams have been obtained by the topological method in combination with experimental data under pressure, such as with high-pressure thermal analysis.[3,6,12-15]

In addition to the Clapeyron equation (Eq. 1), the topological method makes use of the coordinates of triple points. At these points, three phases are in equilibrium with each other. This implies that three two-phase equilibria must cross through a triple point, one for each combination of two phases (for phases I, II, and L for example: I-II, I-L, and II-L). Thus if the coordinates are known of all triple points, all two-phase equilibria can be placed in the diagram by approximating them by straight lines. The number of triple points in a phase diagram is determined by the number of phases considered. For four phases, four triple points must exist reflecting the four possible combinations (for phases I, II, L (Liquid), and V (Vapour): I-II-L, I-II-V, I-L-V, and II-L-V), for more phases the number of triple points increases rapidly, as determined by Riecke in 1890.[16] In first approximation, two-phase equilibrium curves can be represented by straight lines, because the curves are monotonously increasing functions and the two-phase equilibria can only cross once.[17]

It is relatively easy to find triple point coordinates, once one realizes that the dead volume of a capsule used for thermal analysis should in principle be filled with the vapour of the substance in the capsule. This implies that if a solid melts, it does so in the presence of its vapour phase. Considering that the dead volume is rather small, equilibrium between a solid phase and its vapour phase will have been established relatively quickly. The melting transition is under these conditions (i.e. in a closed thermal analysis capsule) an equilibrium between a solid, a liquid, and their vapour. In other words, one obtains the temperature of the triple point solid-L-V. The same is valid for solid-solid transitions obtained by calorimetry.

Unfortunately, in the case that an inert gas surrounds the system, it is often misunderstood what the actual thermodynamic pressure of the system is and this actually reflects often-occurring experimental conditions. With this in mind the term "ordinary conditions" is defined here to indicate that the system under consideration is in thermal equilibrium with its surroundings and that it has basically saturated its close surroundings with its vapour phase, which is considered in equilibrium with the condensed phase. The term "ordinary conditions" also indicates that the thermodynamic pressure of the system is equivalent to its own (partial) vapour pressure; the presence of an inert gas does not in first approximation affect the vapour pressure of the condensed phase.[18] The total pressure of the gas phase, which in the presence of inert gases will differ from the thermodynamic pressure of the system and which only depends on the temperature, is the sum of the pressures that the individual gases have in vacuum at the given temperature (Dalton's and Gay-Lussac's experiments).[19] Because most organic substances and in particular pharmaceuticals have sublimation pressures that are far below 1 atm, their thermodynamic pressure will be considerably lower than 1 atm even if left in the open air. At ambient temperature (or below), the thermodynamic pressure of the system will therefore only equal 1 atm, if the system, exclusively consisting of condensed phases, is subjected to a hydrostatic pressure.[20,21]

L-Tyrosine ethyl ester

L-Tyrosine ethyl ester (L-TEE) has been studied with synchrotron X-ray diffraction in the framework of a much larger study on the behaviour of pharmaceuticals under the influence of pressure. Previously, L-TEE was found to exhibit dimorphism and two crystal structures have been reported.[12,22,23] Both structures have an orthorhombic unit cell with space group $P2_12_12_1$, although the conformation of the ester group is very different in the two crystal structures, a common feature in organic molecules.[24-29] The polymorph that possesses a stable melting transition at 376.4 K is called form I.[12] This is

also the commercial form. Polymorph II transforms into form I at 306 K, thus just above room temperature.[12] In the remainder of the text the solid form I will be designated by I or form I, the solid form II by II, the liquid of L-TEE by L, and its gas phase or vapour phase by V.

In the case of L-TEE form I, the solid-liquid or melting equilibrium was obtained by high-pressure thermal analysis and the melting pressure (MPa) as a function of the temperature (K) is given by:[12]

I-L: $P = 16227 - 91.6\,T + 0.129\,T^2$ (Eq. 2)

The vapour pressure of the liquid phase (P_L (Pa)) has been approximated by the following expression:[12]

L-V: $$\ln\left(P_L\right) = \frac{-\Delta_{L\rightarrow V}H}{RT} + B_{L\rightarrow V} = \frac{-64.69}{RT} + 24.7$$ (Eq. 3)

With $\Delta_{L\rightarrow V}H$ the enthalpy of vaporization, R the gas constant (8.3145×10^{-3} kJ mol^{-1} K^{-1}), T the temperature in kelvin, and $B_{L\rightarrow V}$ an integration constant (integrating the Clapeyron equation). From Eq. 3, the following expression was derived for the vapour pressure (Pa) of form I:[12]

I-V: $$\ln\left(P_I\right) = \frac{-\Delta_{I\rightarrow V}H}{RT} + B_{I\rightarrow V} = \frac{-96.54}{RT} + 34.9$$ (Eq. 4)

These equations can be used for the construction of a topological phase diagram as they represent the two-phase equilibria I-L (Eq. 2), L-V (Eq. 3), and I-V (Eq. 4) and may be used to calculate the triple point coordinates.

In the present paper, a new solid phase of L-TEE and its structure will be presented, which has been discovered by synchrotron X-ray diffraction, while applying pressure to the commercial form I. A topological phase diagram has been constructed including

form I, the new solid phase, the liquid phase, and the vapour phase. In addition, the Clapeyron equation will be used to obtain calorimetric information from otherwise purely crystallographic measurements.

Experimental

L-Tyrosine ethyl ester

L-Tyrosine ethyl ester (M = 209.24 g mol^{-1}) was purchased from Sigma–Aldrich (Saint-Quentin Fallavier, France) (99%) and used as provided.

Synchrotron X-ray diffraction

Diffraction data were collected at the high-pressure diffraction beam line Psiché at the synchrotron Soleil (Saclay, France). The samples were loaded in a membrane diamond anvil cell. The pressure was monitored with a ruby and silicon oil was used as the pressure-transmitting medium. The diffraction data were obtained in two separate experiment runs with different wavelengths: 0.4499 and 0.4859 Å. The temperature was controlled with a liquid-nitrogen cryostat and an in-house constructed heater. Diffraction images were treated with the program fit2D.[30] Measurements have been carried out by varying the pressure at a set temperature (250 K, 294 K, 323K, and 337 K, and a few measurements at 303 K). The sample was allowed to equilibrate before each measurement for about 15 minutes, which was extended to 1 hour at 250 K.

Laboratory X-ray diffraction

High-resolution X-ray powder diffraction patterns were obtained overnight for a sample of L-TEE form I at 100 K with a CPS120 diffractometer from INEL (France). It was equipped with a liquid nitrogen 700 series Cryostream Cooler from Oxford Cryosystems (Oxford, UK). Data were collected for about 1 hour per diffraction pattern to monitor a possible phase change.

Structure solution from powder diffraction

The crystal structure of a new crystalline form has been determined with synchrotron X-ray powder diffraction data obtained at 323 K and 580 MPa. For the structure solution, the program *DASH*[31] was employed and the powder pattern was truncated to 9.4° in 2θ (synchrotron: λ = 0.4499 Å), corresponding to a real-space resolution of 2.75 Å. The background was subtracted with a Bayesian high-pass filter.[32] Peak positions for indexing were obtained by fitting with an asymmetry-corrected pseudo-Voigt function.[33,34] Twenty peaks were indexed with the program *DICVOL*06.[35,36] An orthorhombic unit cell was obtained. The figures of merit given by *DICVOL* were M(20) = 10.3 and F(20) = 68.5 (0.0066, 44). Pawley refinement was used to extract integrated intensities and their correlations, from which the space group was determined using Bayesian statistical analysis.[37] $P2_12_12_1$ was returned as the fourth most probable space group after the extinction symbols *P*ca-, *P*na-, and *P*ba-. Attempts to find a crystal structure with space groups related to the first three extinction symbols did not lead to acceptable solutions, whereas $P2_12_12_1$ did. Moreover, the structure of L-TEE form I possesses the same space group and all other tyrosine alkyl esters too.[23] The space group $P2_12_12_1$ contains no improper symmetry elements, consistent with the crystal structure of an enantiomerically pure compound. It resulted in a Pawley χ^2 of 6.12. Simulated annealing was used to solve the crystal structure from the powder pattern in direct space. The starting molecular geometry was taken from the published form II from the CSD (reference code XAVVIB).[12] In first instance, a plausible structure similar to form I was frequently found but the profile χ^2 remained high at around 44. Adding preferential orientation along a* (1,0,0) improved the profile χ^2 considerably. In 30 simulated annealing runs, the same crystal structure was found 25 times. The profile χ^2 of the best solution was 19.25, which is about three times the Pawley χ^2; this is a good indication that the correct solution has been found. In addition, the structure was very similar to phase I, which made a pressure induced transition likely.

For the Rietveld refinement, data out to 15.9° 2θ were used, which corresponds to 1.63 Å real-space resolution. The Rietveld refinement was carried out with *TOPAS-Academic*.[38] Bond lengths, bond angles and planar groups were subjected to suitable restraints, including bonds to H atoms. A global B_{iso} was refined for all non-hydrogen atoms, with the B_{iso} of the hydrogen atoms constrained at 1.2 times the value of the global B_{iso}. The inclusion of a preferred-orientation correction with the March-Dollase formula[39] was tried and both the preferred-orientation correction for the (211) and the (131) direction made a significant difference to the R_{wp} value. The molecular geometry was checked with *Mogul*,[40] which compares each bond length and bond angle to corresponding distributions from single-crystal data.

Supplementary crystallographic data can be found in the CCDC, deposit number 1045260, and obtained free of charge from the Cambridge Crystallographic Data Centre via www.ccdc.cam.ac.uk/data_request/cif/.

Results

X-ray diffraction patterns as a function of pressure and temperature

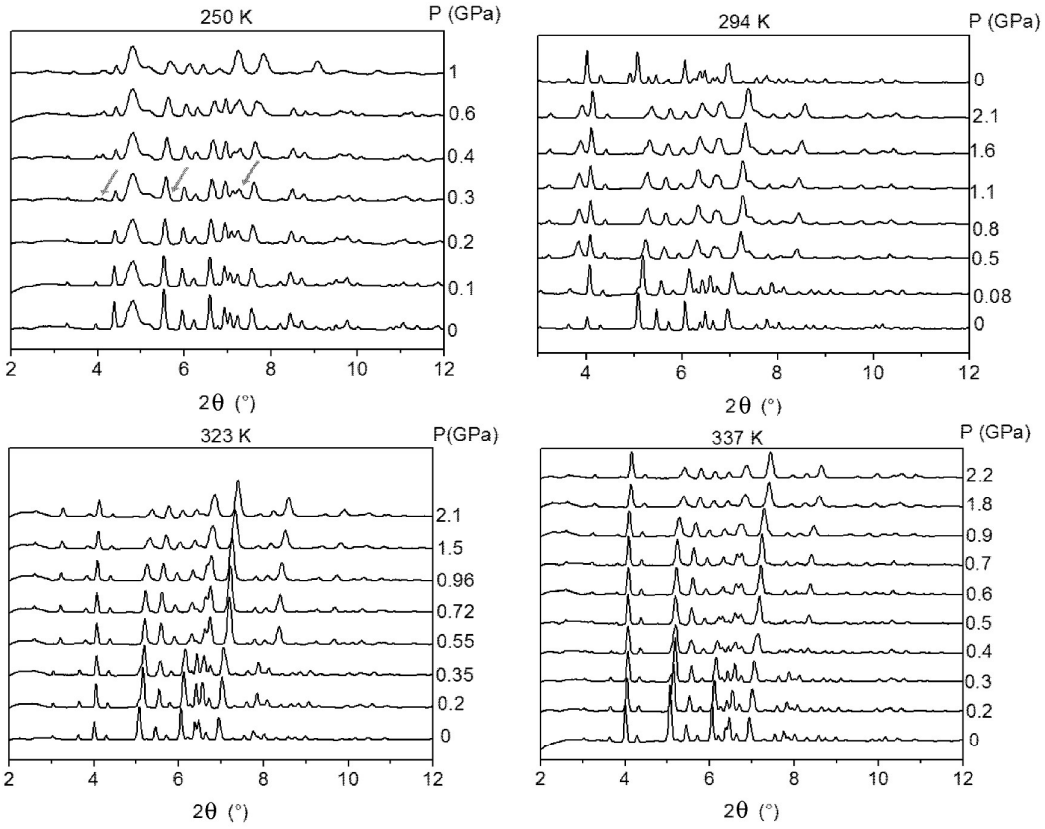

Figure 1. Diffraction patterns of L-TEE as a function of pressure for form I at 250 K (top left), 294 K (top right), 323 K (bottom left) and 337 K (bottom right). The measurement sequences, shifted for clarity, start at the bottom and end at the top in each individual graph.

In Figure 1 for each measurement temperature, the diffraction patterns of L-TEE form I have been provided as a function of pressure. It can be seen that the diffraction pattern of form I changes between 0.3 and 0.5 GPa at 294 K, indicating a structural change in the system. This structural change remains at least up to 2.1 GPa (at 294 K), but the system reverts back to the initial structure, when the pressure is released (The diffraction pattern marked with 0 GPa above that of 2.1 GPa was obtained after the pressure was released (294 K)). Comparison of the new diffraction pattern with the other known crystal structure of L-TEE, form II, reveals that the diffraction pattern obtained under

pressure is different, therefore the solid phase represented by the new diffraction pattern will be called form III from here on.

The transformation of form I into form III can also be observed at the other measurement temperatures, however, the pressure at which the new form appears changes. This can be seen in Figure 2 where, with increasing pressure, the highest pressures at which form III is not observed are marked by circles and the lowest pressures at which form III is observed are marked by squares. The lower the temperature, the slower is the transition from form I into form III; thus even though form III was observed at 0.3 GPa for 250 K, it was still mixed with form I. Nonetheless, from a thermodynamic point of view, it indicates that form III under those conditions is more stable than form I, otherwise it would not be possible for form III to appear. On the other hand, it cannot be stated with certainty that form I is the more stable form at 0.2 GPa at 250 K, because the transition into form III may have been too slow to observe. Unfortunately, control over the pressure in the diamond-anvil cell was limited on descent, in particular at low temperature and low pressure, and an accurate pressure at which form I reappeared could not be determined. Although approximate, the dependence on the pressure and temperature of the transition of form I into form III is clear: with increasing temperature the transition pressure increases or in other words, the slope of the I-III equilibrium in a pressure – temperature phase diagram is positive. This is an important element for the construction of the complete topological phase diagram containing the three observed solid phases, I, II, and III, the liquid and the vapour phase.

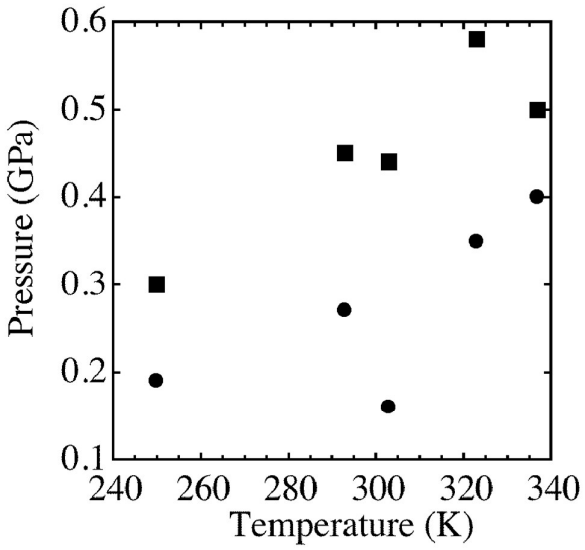

Figure 2. The observations of form III as a function of temperature and pressure, solid circles: maximum pressure at which form III is not observed with increasing pressure, solid squares: minimum pressure for which diffraction peaks of form III have been observed with increasing pressure.

An attempt to obtain form III under ordinary pressure

The synchrotron data in Figure 2 lead to the inference that at very low temperatures form III would become stable under its own vapour pressure, i.e. under ordinary conditions. Therefore form I was monitored overnight at 100 K (the lowest possible temperature for the laboratory X-ray equipment) for any visible phase change. None was observed. However, the synchrotron data also indicated that with decreasing temperature, in particular for 293 and 250 K, the transition from form I into form III with increasing pressure became consistently slower. It may therefore be possible that the absence of an observation of form III is due to kinetic reasons, instead of thermodynamic reasons. Therefore in the discussion below only the synchrotron data will be taken into account, where both form I and form III as a function of pressure have been observed; however, in the electronic supplementary information an alternative calculation will demonstrate the effect on the phase diagram if form I is considered to be stable at 100 K.

The structure of form III

The procedure for the structure solution has been described in the experimental section. The Rietveld refinement progressed smoothly and produced a good fit with χ^2 = 2.624, R'_p = 9.589, R'_{wp} = 13.886 (values after background correction), R_p = 6.491 and R_{wp} = 13.003 (values before background subtraction). The background of the signal was very large and curved, which complicated the fitting of the background of the diffraction pattern and caused the relatively high R-values. The March-Dollase parameter for the (211) direction refined to a value of 2.10(8) and that for the (131) direction to 0.67(1) with a fraction for the first value of 0.49(3); B_{iso} refined to 5.6(4) Å^2.

The cell parameters of form III can be found in Table 1. The structure is orthorhombic, space group $P2_12_12_1$ and a unit-cell volume of 1057.6(5) Å^3. The conformation is shown in Figure 3a, the result of the Rietveld refinement in Figure 3b and the crystal packing in Figure 4 (In Figure ESI.3, the calculated diffraction patterns of form III and form I have been provided in the same graph for comparison).

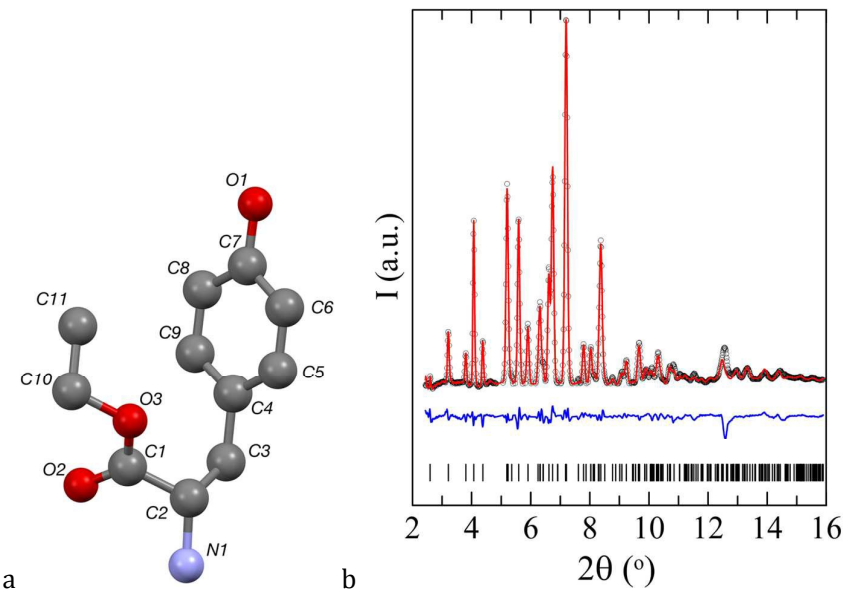

Figure 3. (a) The conformation of L-TEE form III at 323K and 0.58 GPa with atom labels (hydrogen atoms omitted for clarity). **(b)** Result of the Rietveld refinement against the powder diffraction pattern collected at

323 K and 0.58 GPa (open circles: data, red line: fit, blue line: residuals, vertical lines: calculated Bragg peak positions).

Table 1. Crystal data and structure refinement of l-tyrosine ethyl ester form III

Crystal data	***Refinement***
$C_{11}H_{15}O_3N$	Refinement on I_{net}
M_r = 209.24 g mol^{-1}	R_p = 6.491
Orthorhombic, $P2_12_12_1$	R_{wp} = 13.003
a = 12.655(4) Å	R_{exp} = 4.954
b = 16.057(4) Å	χ^2 = 2.624
c = 5.2046(12) Å	Profile function: modified Thompson-Cox-Hastings pseudo-Voigt
V = 1057.6(5) Å^3	192 reflections
Z = 4	133 parameters
Synchrotron radiation 0.4499 Å	81 restraints
T = 323 K, P = 0.58 GPa	H-atom parameters restrained
Data collection	Weighting scheme based on measured s.u.'s $w = 1/\sigma(Y_{obs})^2$
Diffractometer Psiché at synchrotron Soleil	$(\Delta/\sigma)_{max}$ = 0.001
Specimen mounting: diamond anvil cell	Preferred orientation correction: March-Dollase with directions (211) and (131) and March-Dollase
Absorption correction: none	
$2\theta_{min}$ = 0.1°, $2\theta_{max}$ = 37.5°	

parameters of 2.10(8) and 0.67(1) respectively with the ratio 0.49(3)/0.51(3).

Discussion

Comparison of the structures of form I and form III

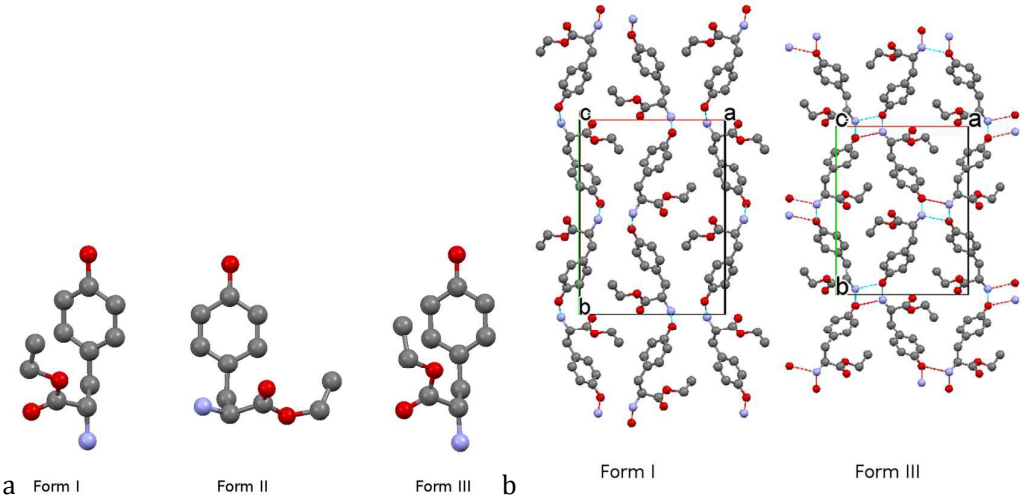

Figure 4. **(a)** Conformations of L-TEE in its three known polymorphs **(b)** Packing of L-TEE form III compared to that of form I, the dotted lines are hydrogen bonds, H atoms have been omitted for clarity.

L-TEE molecules in form III and form I have approximately the same U-shape (or scorpion-like) conformation. The main difference is the orientation of the carboxylate group. A rotation of about 15° around the C(1)-C(2) bond exists (Table 2, torsion O(2)-C(1)-C(2)-N(1)), which is clearly linked to the shift and strengthening of the hydrogen bonds. In addition, the ester group has rotated for about 15° around the O(3)-C(1) bond (Table 2, torsion C(10)-O(3)-C(1)-C(2)).

Table 2. Selected torsion angles of L-TEE form III and form I[a]

Torsion angle (°)	form I[22]	form III
C(2)-C(3)-C(4)-C(5)	+70.63(3)	+81.2(4)
C(2)-C(3)-C(4)-C(9)	-108.06(2)	-99.3(4)
C(10)-O(3)-C(1)-C(2)	170.68(2)	-174.5(4)
C(10)-O(3)-C(1)-O(2)	-5.40(3)	-0.4(9)
O(2)-C(1)-C(2)-C(3)	+80.75(3)	+99.5(7)
O(3)-C(1)-C(2)-C(3)	-95.45(2)	-86.4(5)
O(2)-C(1)-C(2)-N(1)	-41.92(3)	-26.0(8)
O(3)-C(1)-C(2)-N(1)	+141.88(2)	+148.0(5)
N(1)-C(2)-C(3)-C(4)	-179.84(2)	-179.6(3)
C(1)-C(2)-C(3)-C(4)	+59.71(2)	+53.5(4)

[a] The torsion angles of form II have been reported previously.[12]

The packing of form III is very similar to that of form I (Figure 4b). Both structures exhibit undulating infinite chains of strong hydrogen bonds parallel to the *b* axis with graph set notation C^1_1 (9).[41] In form I, the chain consists of hydrogen bonds between the OH of the phenol group and the nitrogen of the amino group. In form III, the conformation of the ester has shifted and an additional strong hydrogen bond exists in form III interconnecting the C^1_1 (9) chains along *b* (Table 3) resulting in a second undulating infinite chain C^1_1(9) approximately along the *a* axis (Figure 4b). The two infinite chains in form III create a 3D network.

Table 3. Hydrogen bonds in form III and close contacts

D-H···A	D-H	H···A	D···A	D-H···A	Graph set Level 1
O1-H1···N1	0.976(16)	2.013(16)	2.839(6)	164.1(1.3)	$C^1_1(9)$//b
N1-H···O1	0.989(15)	1.741(15)	2.678(6)	156.7(1.3)	$C^1_1(9)$//a
C2-H2···O1	0.950(12)	3.617(15)	3.606(6)	81.8(9)	
C10-H10b···O2	0.952(17)	3.053(17)	3.404(9)	103.6(1.1)	

To compare the intermolecular interactions of forms I and III, Hirshfeld surfaces have been constructed (Figure ESI.1). Fingerprint plots are provided for easy comparison between the two structures (Figure 5). In form I the strongest hydrogen bond obviously forms the $C^1_1(9)$ chain along *b*. The weaker hydrogen bond between the nitrogen hydrogen and hydroxyl oxygen atom can also be seen as separate peaks in the fingerprint plots, just next to the stronger H···N interaction (Figure 5).[23] The H···O interactions are not limited to the hydroxyl group but also involve the oxygen atoms of the ester as can be seen in Figure 5. The fingerprint plot of form III is remarkably similar. However, the strongest hydrogen bond now appears to be the one forming the $C^1_1(9)$ infinite chain along *a* as can be seen in Table 3.

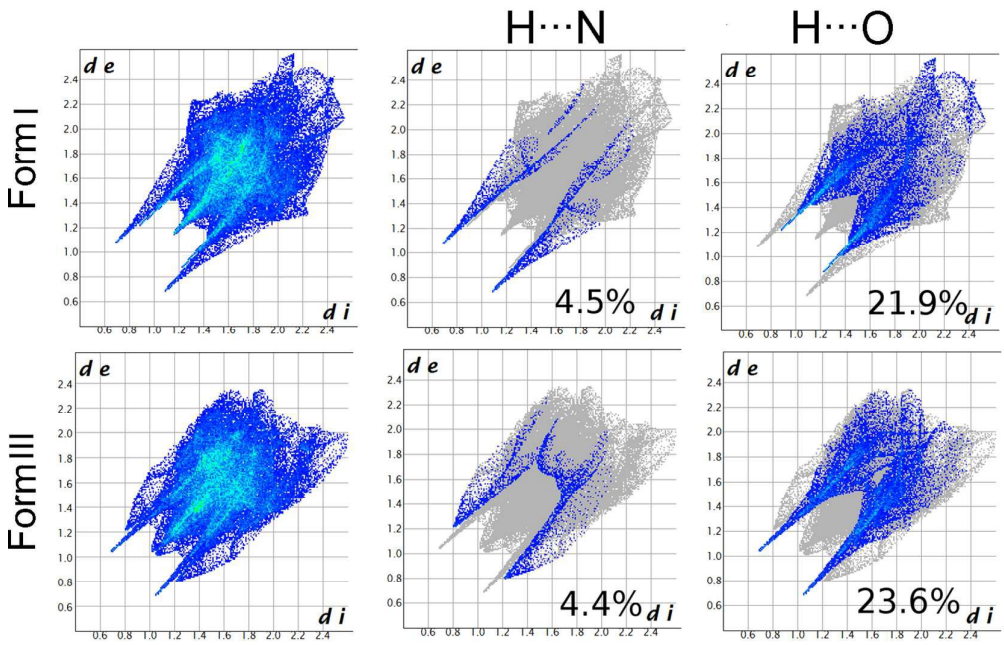

Figure 5. Fingerprint plots for forms I and III with the (d_i, d_e) frequency increasing from deep blue to light blue, left-hand side: all interactions, center: N···H interactions, and right-hand side: O···H interactions.

The phase relationships between the phases I, III, and L

It is clear from the experimental data in this paper that form I turns into form III under pressure. It can also be inferred from Figure 2 that with decreasing temperature the pressure of transition decreases; in other words, the slope of the I-III equilibrium in a pressure-temperature phase diagram, dP/dT, is positive. Form I is more stable below the equilibrium line and form III above this line (see Figure ESI.2a, see for a step-by-step construction of the phase diagram the Electronic Supplementary Information).

Using the data in Figure 2 and fitting the highest observed pressures for form I at 250 K and 337 K, one obtains the expression P (MPa) = – 413 + 2.41 T (K) and fitting the lowest observed pressures for form III at 250 K and 337 K one obtains the expression P = – 275 + 2.30 T. The two slopes are similar and the average slope equals 2.36 MPa K^{-1}. Averaging the two other fitting coefficients results in -344 MPa (at T = 0 K) and leads to the following estimate for the I-III equilibrium line (P in MPa and T in K):

I-III: $P = -344 + 2.36\,T$ (Eq. 5)

Eq. 5 is an estimate; however, it is clear that the slope of the equilibrium is positive, because the pressure at which form I is observed at 337 is higher than the pressure at which form III is observed at 250 K (Figure 1 and Figure 2). The line through the latter two points results in the expression $P = 12.6 + 1.15\,T$, the extreme with the shallowest slope. The other extreme would be fitting a line through the pressure observed for form III at 337 and the pressure for form I observed at 250 K, this leads to the expression $P = -701 + 3.56\,T$. It can be seen that in all cases the slope of the I-III equilibrium line, dP/dT, is positive (see Figures 6 and ESI.2a).

Eq. 5 intersects the temperature axis (P = 0 MPa) at 146 K; hence under ordinary pressure (P equals the vapour pressure of L-TEE ≅ 0 MPa), form III would be stable in relation to form I below 146 K (however, considering the two extremes, this transition at ordinary pressure lies between 197 and 0 K). The difference between form I and form III is a conformational change leading to the formation of an additional strong hydrogen bond.

Taking 293 K for the transition temperature of I-III, as it is in the centre of the temperature interval (250 – 337 K) over which the slope of the equilibrium I-III has been determined, the estimated transition pressure follows from Eq. 5 and equals 346 MPa. With a Pawley refinement, the volume of form I below this pressure can be calculated resulting in 1114 $Å^3$ at 293 K and 270 MPa. For form III at 293 K, the volume can be determined from the diffraction pattern at 450 MPa leading to 1050 $Å^3$. Although the volumes have not been determined at the same pressure, the variation in the volume with the phase change from I to III equals now approximately −64 $Å^3$ (= 9.6 cm^3mol^{-1}). By applying the Clapeyron equation, Eq. 1, using the slope of 2.36 MPa K^{-1} from Eq. 5, the obtained volume difference leads at 293 K to an enthalpy change for the transition of −6.65 kJ mol^{-1}.

The transition from form I to form III is exothermic and the energy of the system decreases. This is consistent with form III being the low temperature form in relation to form I, because the low temperature form should have a lower energy content than the high temperature form as implied by the Le Chatelier principle.

Using the information on the phase behaviour between form I and form III and the previously published melting curve as a function of pressure of form I, Eq. 2,[12] the topological phase diagram of the dimorphism of I and III in combination with the liquid and the vapour phase can be constructed. This diagram (Figure 6) consists of the equilibria between I and III, which is represented by Eq. 5, I and L (Eq. 2), III and L, I and V (Eq. 4), III and V, and finally L and V (Eq. 3). As can be seen, most of the equilibria have already been determined and the text below will focus on the equilibria between III-L, and III-V.

For the III-L equilibrium, the triple point I-III-L can be calculated, at which form III is in equilibrium with form I and L. The triple point coordinates can be obtained by setting Eq. 5 (equilibrium I-III) and Eq. 2 (equilibrium I-L) equal to each other resulting in the coordinates 430 K and 669 MPa (Figures 6 and ESI.2c). Another point on the III-L equilibrium can be obtained by using a formula derived previously, which links the melting points at ordinary pressure of two solid phases with the transition temperature and the enthalpies of those two phases:[6,42]

$$T_{III\rightarrow L} = \frac{\Delta_{I\rightarrow L}H + \Delta_{III\rightarrow I}H}{\left(\Delta_{I\rightarrow L}H / T_{I\rightarrow L}\right) + \left(\Delta_{III\rightarrow I}H / T_{III\rightarrow I}\right)} \qquad \text{(Eq. 6)}$$

$T_{\mathrm{III}\rightarrow\mathrm{L}}$ is the melting temperature of form III at ordinary pressure, $\Delta_{\mathrm{I}\rightarrow\mathrm{L}}H$ is the molar melting enthalpy of form I and so on for the other variables with the arrow indicating the direction of the phase shift. The enthalpy change for the fusion of form I, $\Delta_{\mathrm{I}\rightarrow\mathrm{L}}H$ = 31846 J mol^{-1}, is known from a previous study as is its melting point ($T_{\mathrm{I}\rightarrow\mathrm{L}}$ = 376.42 K).[12]

The enthalpy change of the solid-solid transition III-I has been calculated above and is equal to $\Delta_{III\rightarrow I}H$ = −6652 J mol^{-1}. The temperature for the solid-solid transition at ordinary pressure follows from Eq. 5 and is equal to $T_{III\rightarrow I}$ = 146 K. Using these values the melting point of form III becomes $T_{III\rightarrow L}$ = 296 K. An estimate of the melting enthalpy can be obtained with the thermodynamic cycle III→L→I→III. Because the enthalpy is a state function, the enthalpy difference of this cycle must be zero; thus $\Delta_{I\rightarrow III}H + \Delta_{III\rightarrow L}H = \Delta_{I\rightarrow L}H$. Using the enthalpy values mentioned above, neglecting the heat capacities, the melting enthalpy of form III becomes $\Delta_{III\rightarrow L}H = (\Delta_{I\rightarrow L}H) - (\Delta_{I\rightarrow III}H)$ = 31846 + 6652 = 38498 kJ mol^{-1} or 38.5 kJ mol^{-1}.

The second coordinate of the melting point under ordinary conditions is the vapour pressure of L-TEE. Because $T_{III\rightarrow L}$ is a melting point, the vapour pressure of the liquid must be equal to that of the solid phase III. Thus, using Eq. 3, the vapour pressure of the liquid, P_L (Pa), can be calculated for 296 K (= $T_{III\rightarrow L}$) and is found to be 0.205 Pa. Obviously, this value is so low that it can be safely written as 0 MPa. The two points on the melting equilibrium III-L, triple point III-L-V (296 K, 0 MPa) and triple point I-III-L (430 K, 669 MPa) allow a linear approximation of the melting pressure $P_{III\text{-}L}$ (MPa) as a function of the temperature (K) (see Figure ESI.2d and Figure 6):

III-L: $P = -1475 + 5.0\ T$ (Eq. 7)

It can be seen that the slope of Eq. 7 is intermediate to the slope of the melting equilibrium of form I (6.9 MPa K^{-1} obtained by taking the first three measurement points fitted by Eq. 2) and that of the solid-solid transition I-III (2.36 MPa K^{-1}, Eq. 5).

Eq. 7 is an approximation, because the two triple points are estimates obtained by extrapolation. The melting point of form III at ordinary pressure is based on the estimates of the transition enthalpy between forms I and III and of the I-III transition temperature of 146 K. Nonetheless, it is clear that the enthalpy is positive and that the

transition temperature of form III to form I under ordinary pressure is much lower than the melting point of form I. Moreover, the melting temperature of form III is quite low ($\Delta T \cong 80$ K) with respect to the melting point of form I. It defines the phase behaviour of the two phases III and I as enantiotropic under ordinary pressure, while it turns monotropic at elevated pressure with form III the only stable solid phase. This is schematically demonstrated in Figure 6.

The only expression that is still lacking is the vapour pressure of form III. Although the pressure is very low as is clear from the calculation of the III-L-V triple point above, for the sake of completeness, it will be provided. A general and approximate expression for the vapour phase has been given in Eq. 3 and Eq. 4, which is here rewritten for form III (pressure in Pa, and temperature in K):

III-V: $$\ln\left(P_{III}\right) = \frac{-\Delta_{III\rightarrow V}H}{RT} + B_{III\rightarrow V} = \frac{-103.2}{RT} + 40.4 \qquad \text{(Eq. 8)}$$

The enthalpy of sublimation $\Delta_{III\rightarrow V}H$ can be obtained by adding the enthalpy of fusion of form III, 38.5 kJ mol^{-1} and that of vaporization of the liquid, 64.69 kJ mol^{-1} leading to 103.2 kJ mol^{-1}, because for state functions such as enthalpy the path is not important, only the initial and final state are, here solid III and vapour, respectively. To obtain the value for the constant $B_{III\rightarrow V}$, it should be realized that the vapour pressure of solid III is the same as that of the liquid at its melting point of 296 K. With this known pressure of 0.205 Pa (calculated above for the triple point III-L-V), the value of 40.4 for the constant $B_{III\rightarrow V}$ is obtained.

The topological pressure-temperature phase diagram for the phases III, I, L, and V

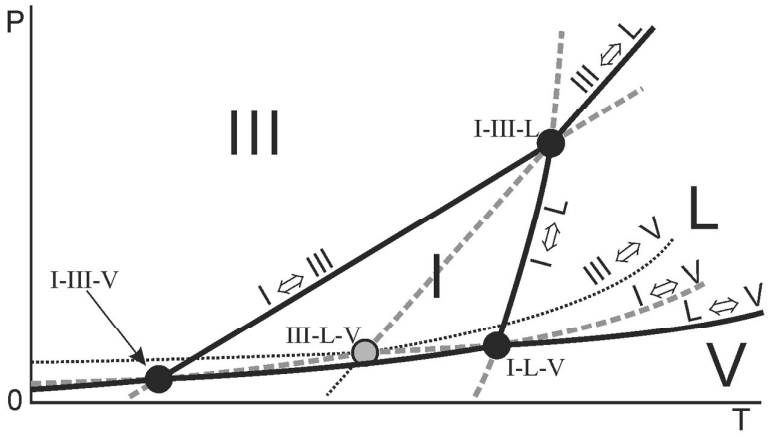

Figure 6. Topological phase diagram of the L-TEE phases I, III, L, and V. Solid black lines: stable phase equilibria for the given set of phases (III, I, L, and V), grey broken lines: metastable equilibria, dotted lines supermetastable equilibria. The solid circles are stable triple points and the grey circle is a metastable triple point (For coordinates see Table 4). The solid black lines surround the domains of the four stable phases as indicated in the diagram: I and III are solid forms I and III, L = liquid, V = vapour, pressure and temperature coordinates are not to scale. A step by step construction of the phase diagram is provided in the electronic supplementary information.

To obtain Figure 6, the relative stabilities of the different phases, the phase equilibria, and the triple points need to be determined. The coordinates of the triple points can be calculated with the equations discussed above. The result can be found in Table 4.

Table 4. Temperature and pressure coordinates of the triple points

Triple point	T (K)	P (Pa)
I-L-V	376.4	57
III-L-V	295.8	0.2
III-I-V	146.0	0

III-I-L	429.9	669 ×10^6

The starting point to determine the stability hierarchy in the phase diagram is the triple point I-L-V, which represents the melting point of form I in the presence of the vapour phase. Because it is the highest melting point in this phase diagram, it must be the most stable one (at least with respect to the solid phase III present), indicated by a solid black circle (marked by I-L-V, Figure 6 and Figure ESI.2a). Following the melting equilibrium I-L upward, only the solid I and the liquid are in equilibrium, however, it is still the highest melting transition at moderate hydrostatic pressure, hence this solid black line represents the more stable equilibrium under the given conditions. Necessarily, the triple point I-III-L is also stable, as it includes the stable melting equilibrium of form I.

Pressure-temperature phase diagrams are a projection of the intersections of the Gibbs energy surfaces as a function of pressure and temperature. Due to the fact that in a triple point three Gibbs energy surfaces must come together, an equilibrium intersecting a triple point must change its stability hierarchy as on the other side of the triple point the Gibbs energy surface of a different phase will be lower (i.e. another phase will be more stable). As a result, around a triple point, the stability hierarchy will always alternate between two levels of stability. In the case of triple point I-III-L, those levels are stable and metastable. It can be seen that the melting equilibrium I-L becomes metastable after the triple point (Figure 6 and also Figure ESI.2c). Moreover, going clockwise around the triple point, the next equilibrium that is encountered, here III-L must be metastable, because it finds itself in the domain where form I is stable. Continuing clockwise around the triple point equilibrium III-I must be stable again, I-L metastable, III-L stable, and III-I metastable. Although this result is obtained through thermodynamics (Gibbs energy surface intersections), it makes sense intuitively. If I-L is the stable equilibrium at the highest temperature, then a solid melting at a lower temperature cannot be stable.

Furthermore, if I is the stable solid that melts, it must become stable through the III→I transition, which therefore must be stable itself. Going up in pressure, it is form III, which is the stable solid; thus form III will have a stable melting equilibrium. Finally, a solid-solid transition in the domain of a stable liquid can only be metastable. Thus, equilibria I-L and III-I are stable below the triple point and III-L above it.

The same logic can be applied to the other triple points. Taking the stable equilibrium III-I down to low pressure and temperature, it reaches the triple point III-I-V (Figure 6). Obviously, below this triple point the vapour phase is stable and the III-I equilibrium can be but metastable. This also means that at the low-temperature side of the III-I-V triple point, where stable form III and the vapour phase meet, the III-V equilibrium must be stable, and at the high-temperature side of the III-I-V triple point, it is the I-V equilibrium that is stable (Figure ESI.2b). It can also be observed that all equilibria remain present throughout the diagram, but with different stability levels i.e. different Gibbs energies.

One triple point in this diagram is metastable (grey circle), and this is the melting point of form III under ordinary conditions in equilibrium with the vapour phase. Because in this case no stable equilibria intersect the triple point, the alternation of the hierarchy involves metastable and supermetastable equilibria, which possess thus even higher Gibbs energy levels. Finally, at the stable melting point of form I under ordinary conditions, it is clear that the three stable equilibria are I-L, L-V (the vapour pressure curve of the liquid), and I-V (the vapour pressure curve of solid I). The solid black lines in Figure 6, connected by the solid black circles divide the phase diagram up into four domains constituting the conditions in which one of the four phases III, I, L, or V are stable.

The result in Figure 6 is a topological phase diagram based in the case of form III solely on the synchrotron data. The synchrotron data lead to an expression for the III-I

equilibrium line that cuts the 0 MPa coordinate at 146 K, whereas laboratory experiments with a powder diffractometer did not lead to the observation of form III at 100 K. Unfortunately, the absence of the observation of form III does not necessarily mean that form III is not stable at 100 K. It may mean that the transition at 100 K is too slow to be observed. 100 K was the lowest temperature limit for controlled measurements with the X-ray diffractometer and possibly a measurement at an even lower temperature would lead to the observation of a lower transition temperature, but for now in absence of such an observation, only the synchrotron data have been used because the transition could be observed as a function of pressure. It is of course possible to incorporate the non-observation of form III at 100 K as a measurement point, which would imply that the transition III-I must lie at an even lower temperature. The values for the triple points one would obtain in that case have been provided in the Electronic Supplementary Information. Nonetheless, the topological layout of the phase diagram, case 1 of the four possible phase diagrams for dimorphism published in 1901 by Bakhuis-Roozeboom[13,43] and depicted in Figure 6 will not change.

Conclusions

The phase behaviour of simple chemical compounds like L-tyrosine ethyl ester remains surprising. Applying pressure to form I causes a small conformational change in the ethyl tail of the ester and enables the formation of an additional hydrogen bond. The space group of the unit-cell is $P2_12_12_1$ like form I and all the other unit cells in the L-tyrosine ester series.[12,22,23,44]

Even though form III is only found under pressure, the diffraction data indicate that the dP/dT slope of the III-I equilibrium is positive and that this equilibrium will reach ordinary pressure (≈ 0 MPa) somewhere between 200 and 0 K. Experiments at 100 K under ordinary pressure were not conclusive as form III has not been observed. It was

already clear from the synchrotron measurements that the transition becomes slower with decreasing temperature. It is therefore not known whether the absence of form III was due to the freezing in of a metastable system or due to a higher stability of form I relative to form III at 100 K. It is clear however, that the III-I equilibrium at ordinary pressure will occur far below room temperature.

The analysis has led to a topological phase diagram, which implies that the coordinates of the triple points and the equilibrium lines obtained through inter- and extrapolation are approximate. However, the position of the different stability domains relative towards each other, form III being a high-pressure, low-temperature form and form I being a low-pressure, high-temperature form will not change with additional data.

Despite the fact that the precise location of the III-I equilibrium could not be determined, the estimate of the slope obtained by the synchrotron data leads to the enthalpy change of the III-I transition using the volume change obtained from the diffraction profiles. The enthalpy change in the order of 6 kJ mol^{-1} is clearly in the range expected for a solid-solid transition and is the sum of the energy necessary for a small conformational change and for the strengthening of a hydrogen bond. Thus with the Clapeyron equation, calorimetric data can be obtained through X-ray diffraction obtained under pressure.

Electronic Supplementary Information. Alternative calculation of equilibrium lines and triple points taking into account the laboratory observations at 100 K. Table with alternative triple point coordinates. Figure with Hirshfeld surfaces of form I and form III. Figures demonstrating the schematic construction of the topological phase diagram. A figure with the calculated powder diffraction patterns of form I and form III.

References

(1) Neumann, M. A.; Perrin, M. A., *CrystEngComm* **2009,** 11, 2475-2479.
(2) Espeau, P.; Ceolin, R.; Tamarit, J. L.; Perrin, M. A.; Gauchi, J. P.; Leveiller, F., *J. Pharm. Sci.* **2005,** 94, 524-539.
(3) Ledru, J.; Imrie, C. T.; Pulham, C. R.; Ceolin, R.; Hutchinson, J. M., *J. Pharm. Sci.* **2007,** 96, 2784-2794.
(4) Ceolin, R.; Rietveld, I. B., *J. Therm. Anal. Calorim.* **2010,** 102, 357-360.
(5) Barrio, M.; Maccaroni, E.; Rietveld, I. B.; Malpezzi, L.; Masciocchi, N.; Ceolin, R.; Tamarit, J.-L., *J. Pharm. Sci.* **2012,** 101, 1073-1078.
(6) Gana, I.; Barrio, M.; Do, B.; Tamarit, J.-L.; Ceolin, R.; Rietveld, I. B., *Int. J. Pharm.* **2013,** 456, 480-488.
(7) Gana, I.; Ceolin, R.; Rietveld, I. B., *J. Therm. Anal. Calorim.* **2012,** 112, 223-228.
(8) Gana, I.; Ceolin, R.; Rietveld, I. B., *Thermochim. Acta* **2012,** 546, 134-137.
(9) Gajda, R.; Katrusiak, A.; Crassous, J., *CrystEngComm* **2009,** 11, 2668-2676.
(10) Rietveld, I. B.; Ceolin, R., *J. Therm. Anal. Calorim.* **2015**, DOI: 10.1007/s10973-014-4366-2
(11) Ceolin, R.; Rietveld, I. B., *Ann. Pharm. Fr.* **2015,** 73, 22-30.
(12) Rietveld, I. B.; Barrio, M.; Tamarit, J.-L.; Nicolai, B.; Van de Streek, J.; Mahe, N.; Ceolin, R.; Do, B., *J. Pharm. Sci.* **2011,** 100, 4774-4782.
(13) Ceolin, R.; Tamarit, J. L.; Barrio, M.; Lopez, D. O.; Nicolaï, B.; Veglio, N.; Perrin, M. A.; Espeau, P., *J. Pharm. Sci.* **2008,** 97, 3927-3941.
(14) Perrin, M.-A.; Bauer, M.; Barrio, M.; Tamarit, J.-L.; Ceolin, R.; Rietveld, I. B., *J. Pharm. Sci.* **2013,** 102, 2311-2321.
(15) Négrier, P.; Barrio, M.; Tamarit, J. L.; Mondieig, D.; Zuriaga, M. J.; Perez, S. C., *Cryst Growth Des* **2013,** 13, 2143-2148.
(16) Riecke, E., *Z. Phys. Chem. (Munich)* **1890,** 6, 411.
(17) Oonk, H. A. J., *Phase theory, The thermodynamics of heterogeneous equilibria*. ed.; Elsevier Scientific Publishing Company: Amsterdam, 1981.
(18) Bancroft, W. D., *J. Phys. Chem.* **1897**, 6.
(19) Gibbs, J. W., *The collected works of J.W. Gibbs - Volume 1: Thermodynamics*. ed.; Green&Co: NY, 1928; p 154-160.
(20) Reisman, A., *Phase equilibria - Basic principles, applications, experimental techniques*. ed.; Academic Press: NY, 1970; p 39.
(21) Bridgman, P. W., *Phys. Rev.* **1914,** 3, 126.
(22) Pieret, A. F.; Durant, F.; Griffé, M.; Germain, G.; Debaerdemaeker, T., *Acta Crystallogr. Sect. B: Struct. Sci.* **1970,** 26, 2117-2123.
(23) Nicolai, B.; Mahe, N.; Ceolin, R.; Rietveld, I.; Barrio, M.; Tamarit, J., *Struct. Chem.* **2011,** 22, 649-659.
(24) Rosado, M. T. S.; Maria, T. M. R.; Castro, R. A. E.; Canotilho, J.; Silva, M. R.; Eusebio, M. E. S., *CrystEngComm* **2014,** 16, 10977-10986.
(25) Kumar, S. S.; Nangia, A., *CrystEngComm* **2013,** 15, 6498-6505.
(26) Minkov, V. S.; Boldyreva, E. V.; Drebushchak, T. N.; Gorbitz, C. H., *CrystEngComm* **2012,** 14, 5943-5954.
(27) Thomas, L. H.; Craig, G. A.; Gutmann, M. J.; Parkin, A.; Shankland, K.; Wilson, C. C., *CrystEngComm* **2011,** 13, 3349-3354.
(28) Nowicki, W.; Olejniczak, A.; Andrzejewski, M.; Katrusiak, A., *CrystEngComm* **2012,** 14, 6428-6434.
(29) Bujak, M.; Bläser, D.; Katrusiak, A.; Boese, R., *Chem. Commun.* **2011,** 47, 8769-8771.
(30) Hammersley, A. *Fit2D*, v12.077; http://www.esrf.eu/computing/scientific/FIT2D/fit2d_abstract.html: ESRF, 1987-2005.

(31) David, W. I. F.; Shankland, K.; van de Streek, J.; Pidcock, E.; Motherwell, W. D. S.; Cole, J. C., *J. Appl. Crystallogr.* **2006,** 39, 910-915.
(32) David, W. I. F.; Sivia, D. S., *J. Appl. Crystallogr.* **2001,** 34, 318-324.
(33) Finger, L. W.; Cox, D. E.; Jephcoat, A. P., *J. Appl. Crystallogr.* **1994,** 27, 892-900.
(34) Thompson, P.; Cox, D. E.; Hastings, J. B., *J. Appl. Crystallogr.* **1987,** 20, 79-83.
(35) Boultif, A.; Louer, D., *J. Appl. Crystallogr.* **1991,** 24, 987-993.
(36) Boultif, A.; Louer, D., *J. Appl. Crystallogr.* **2004,** 37, 724-731.
(37) Markvardsen, A. J.; David, W. I. F.; Johnson, J. C.; Shankland, K., *Acta Crystallogr. A* **2001,** 57, 47-54.
(38) Coelho, A. A. *TOPAS Academic version 4.1 (Computer Software)*, Coelho Software: Brisbane, 2007.
(39) Dollase, W. A., *J. Appl. Crystallogr.* **1986,** 19, 267-272.
(40) Bruno, I. J.; Cole, J. C.; Kessler, M.; Jie, L.; Motherwell, W. D. S.; Purkis, L. H.; Smith, B. R.; Taylor, R.; Cooper, R. I.; Harris, S. E.; Orpen, A. G., *J. Chem. Inf. Comput. Sci.* **2004,** 44, 2133-2144.
(41) Etter, M. C., *Acc. Chem. Res.* **1990,** 23, 120-126.
(42) Yu, L., *J. Pharm. Sci.* **1995,** 84, 966-974.
(43) Bakhuis Roozeboom, H. W., *Die heterogenen Gleichgewichte vom Standpunkte der Phasenlehre. Erstes Heft: Die Phasenlehre - Systeme aus einer Komponente.* ed.; Friedrich Vieweg und Sohn: Braunschweig, 1901; Vol. 1.
(44) Qian, S.-S.; Zhu, H.-L.; Tiekink, E. R. T., *Acta Crystallogr. E* **2006,** 62, o882-o884.

Graphical Abstract

Thermodynamics by synchrotron X-ray Diffraction: Phase relationships and crystal structure of L-tyrosine ethyl ester form III

Béatrice Nicolaï, Jean-Paul Itié, Maria Barrio, Josep-Lluis Tamarit, Ivo B. Rietveld

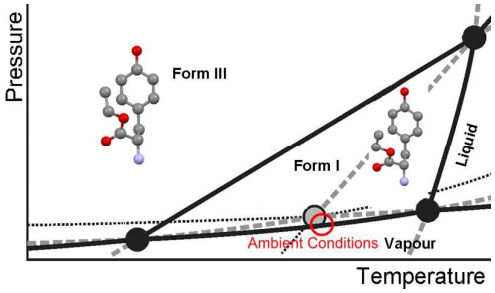

Structure, transition enthalpy and equilibrium curve were obtained by X-ray diffraction for the commercial form and a new crystalline high-pressure form.